EUROPEAN ORGANIZATION FOR NUCLEAR RESEARCH

CERN/EP 89-58
25 April 1989

VECTOR MESON PRODUCTION IN π^-p INTERACTIONS AT 360 GeV/c

LEBC – EHS Collaboration

M.Aguilar-Benitez[6], J.L.Bailly[7], A.A.Batalov[13], E.Castelli[16], P.Checchia[9], P.V. Chliapnikov[13], N.Colino[6], R.Contri[5], A.DeAngelis[9], A.DeRoeck[1], N.DeSerjis[11], J.Duboc[10], A.M.Endler[12], P.F.Ermolov[8], S.Falciano[11], Y.V.Fisjak[13], F.Fontanelli[5], S.Ganguli[3], U.Gasparini[9], S.Gentile[11], Y.A.Golubkov[8], A. Gurtu[3], J.J.Hernandez[6], S.O.Holmgren[15], J.Hrubec[17], M.Iori[11], K.E.Johansson[15], M.I.Josa[6], E.P.Kistenev[13], M.Mazzucato[9], A.Michalon[14], A.Michalon-Mentzer[14], L.Montanet[4], R.Monge[5], H.K.Nguyen[10], H. Nowak[2], L.C.Oliveira[12], V.M.Perevoztchikov[13], P.Pilette[7], P.Poropat[16], A.Poppleton[4], H.Rohringer[17], J.M.Salicio[6], S.Saran[3], M.Sessa[16], E.K.Shabalina[8], F.Simonetto[9], N.A.Sotnikova[8], S.Squarcia[5], V.A.Stopchenko[13], U.Trevisan[5], C.Troncon[16], F.Verbeure[1], J.V.Yarba[8], and G.Zumerle[9]

ABSTRACT

The inclusive production of vector mesons (charged $\rho(770)$, $\omega(783)$, $\phi(1020)$ and neutral $K^*(892)$) in π^-p interactions at 360 GeV/c is studied. The data are based on 160 000 reconstructed events recorded in the NA27 Experiment using the LEBC-EHS facility at CERN. The production cross section in the forward hemisphere in c.m.s. and the longitudinal and transverse momentum distributions are determined. The results are compared with model predictions and with data obtained at lower energies.

Submitted to Zeitschrift für Physik C

---

1) InterUniversity Institute for High Energies ULB-VUB, Brussels and Department of Physics, Universitaire Instelling Antwerpen, Wilrijk, Bel
2) Institut fur Hochenergiephysik der AdW der DDR, DDR-1615 Berlin-Zeuthen, DDR
3) Tata Institute for Fundamental Research, Bombay, India
4) CERN, European Organization for Nuclear Research, Geneva, Switzerland
5) INFN and University of Genoa, Italy
6) CIEMAT-JEN, Madrid, Spain
7) University of Mons, Mons, Belgium
8) Moscow State University, Moscow, USSR
9) INFN and University of Padova, Padova, Italy
10) LPNHE, University of Paris VI, Paris, France
11) INFN and University of Rome, Rome, Italy
12) Centro Brasileiro de Pesquisas Fisicas, Rio de Janeiro, Brazil
13) Institute for High-Energy Physics, Serpukhov, USSR
14) CRN, High-Energy Phys. Div., and University Louis Pasteur, Strasbourg-C, France
15) Dept. of Physics, University of Stockholm, Stockholm, Sweden
16) Institute for Physics, University of Trieste, Trieste, Italy
17) IHEP, Wien, Austria

1. INTRODUCTION

The underlying dynamics of "low p_T" hadron−hadron interactions at high energy is badly known and raises a series of questions:

- the role and fate of the incident valence quarks in the interactions (do these quarks "remember" that they were originally confined in the same hadron?),
- the parton hadronization into final state particles,
- the ratio of vector to pseudoscalar mesons which are produced in this hadronization,
- the suppression factor for the strange quarks creation,
- the role of the OZI suppression rule in inclusive production.

To answer at least partially these questions, it is important to study the hadrons which are as closely as possible related to the primary (partonic) interaction, i.e. to study the production properties of the parents rather than the daugthers, which mean the study of the production of hadronic resonances rather than their decay products.

It is particularly interesting to study the vector meson production (ρ, ω, K^*, ϕ) since both experimental evidence and spin statistical arguments suggest that they contribute through their decay products

$$(\pi^{\pm}, \pi^0, K^{\pm}, K^0, \overline{K}^0)$$

to a large fraction of the particles finally observed.

To achieve such a program, a number of experimental conditions must be satisfied: a large acceptance of the detectors (to have access to a large fraction of the phase space), good momentum resolution (to obtain a good signal for narrow resonances such as $\omega(783)$ and $\phi(1020)$), π^0 as well as $\pi^{\pm}$ detection (essential for $\rho^{\pm}(770)$ reconstruction) and good particle identification ($K^{\pm}/\pi^{\pm}$ separation for $K^* \to K^{\pm}\pi$ and $\phi(1020) \to K^+K^-$ production). These conditions are fulfilled, to a large extent, by the European Hybrid Spectrometer (EHS) [1] which has been used in the experiment described in this paper.

The experiment was performed at CERN, using the H2 beam of the SPS, EHS and a small liquid hydrogen bubble chamber (LEBC) as target. LEBC−EHS was exposed to a beam of 360 GeV/c π^- ($\sqrt{s}$ = 26 GeV). The data accumulated correspond to a sensitivity of 9 events/μb. Details of the experimental procedure are given in sect. 2.

In sect. 3, we present results obtained on the following reactions:

$$\pi^- p \to \rho^-(770) + X, \tag{1}$$

$$\pi^- p \to \omega(783) + X, \tag{2}$$

$$\pi^- p \to \rho^+(770) + X, \tag{3}$$

$$\pi^- p \to K^{*0}(892) + X, \tag{4}$$

$$\pi^- p \to \overline{K}^{*0}(892) + X, \tag{5}$$

$$\pi^- p \to \phi(1020) + X. \tag{6}$$

For completeness, we recall here the results previously obtained [2] by the same experiment on the reaction

$$\pi^- p \to \rho^0(770) + X. \tag{7}$$

Experimental limitations (mainly due to the difficulties associated with K^0 detection) preclude a detailed analysis of the reactions

$$\pi^- p \to K^{*-}(892) + X, \tag{8}$$

$$\pi^- p \to K^{*+}(892) + X, \tag{9}$$

for which we can only give an upper limit for the cross section.

2. THE EXPERIMENTAL SET − UP AND DATA HANDLING

Details on the experimental set − up of EHS are given in ref. [1]. Briefly, EHS consists of a high resolution bubble chamber, serving both as a target and as a vertex detector, a two − lever − arm spectrometer for momentum analysis, a set of detectors for particle identification (mainly $K^{\pm}$ vs $\pi^{\pm}$ in the present experiment) and gamma detector for detection and reconstruction of π^0, η^0 and η'.

2.1 The trigger

Data acquisition was triggered by a simple interaction trigger [3] demanding three or more hits in each of the two single plane trigger wire chambers positioned just downstream of LEBC. The triggered fraction of the total inelastic cross section (21.6 mb [4]) was found to be (80.3 ± 4.5%) [5].

The trigger losses mainly affect low multiplicity interactions (81%, 60% and 26%, for two −, four − and six − prong events respectively). They are much smaller for eight and ten − prong events and become negligible for higher multiplicities. The information collected on two − prong events is unreliable and will not be used in the following analysis. On the contrary, the information collected on the remaining low multiplicity events (four, six, eight, ten − prong) can be used after adequate normalization to the known topological cross sections [5].

The results presented below correspond to 19.7 mb out of 21.6 mb of inelastic cross section, the difference is caused by the inelastic two − prong interactions (1.5 mb) and to a small fraction of the target diffraction (0.3 mb) excluded from the analysis.

2.2 The reconstruction

The event reconstruction was preceded by film scanning. The scanning information was used to select only those triggers corresponding to a primary interaction within the effective volume of the bubble chamber. During scanning only the primary multiplicity and the coordinates of the primary vertex were recorded since the spectrometer data alone are sufficient to achieve track reconstruction with high efficiency and no additional measurement of the bubble chamber pictures is necessary.

The charged particle geometrical acceptance was $\pm$ 200 mrad vertically (in the bending plane of spectrometer magnets) and $\pm$ 90 mrad horizontally. This corresponds to 100% coverage of the forward centre of mass hemisphere (the "π^- hemisphere", in this experiment, as opposed to the "proton hemisphere" for the target proton backward hemisphere).

The momentum accuracy is $\Delta p/p \cong 1.5\%$ for tracks reconstructed in the first lever-arm ($p < 40$ GeV/c) and reaches $\cong 0.8\%$ for those reconstructed in both lever-arms. The single charged particle reconstruction efficiency depends on $x_F (= p^*\| \ / \ p^*_{max})$ and varies from 70% at $x_F = 0.$ to 90% at $x_F = 1.$

2.3 The charged track identification

The charged particle identification is provided by a large pictorial drift chamber, ISIS, which gives for each crossing track a maximum of 320 ionization measurements (N_s) [6]. From the most probable ionization (I_m), defined by a fit of the (N_s) ionization samplings for a given track to Landau distribution, and the expected ionization (I_h), given a mass hypothesis "h" (h = e, π, K, p)[1], one computes a conditional probability

$$P(I_m|I_h) \equiv P(m|h) \ \frac{1}{\sqrt{2\pi}} \ e^{-\frac{\chi^2}{2}},$$

where

$$\chi^2_h = (\ln (I_m/I_h)/\sigma)^2.$$

The error ($\sigma = \Delta I_m/I_m$) on the ionization depends on the number of the ionization measurements (N_s). Its averaged value for our ISIS selection cut ($N_s > 100$) is equal to $\cong 3.5\%$.

Then using as "a priori" information the fractional yield (P(h; Ω)) of the charged particle "h" known from a previous analysis [7] in a given phase space region (Ω) and Bayes theorem, it is possible to calculate for each track the "a posteriori" probability for the hypothesis "h"

$$P(h|m;\Omega) = \frac{P(m|h) \times P(h;\Omega)}{\sum_h P(m|h) \times P(h;\Omega)}. \qquad (10)$$

The track is considered as being of type "h" if

---

[1] If the difference in the energy detected in the γ-detectors and the momentum reconstructed in spectrometer is larger than 5 s.d. or if the momentum is larger than 40 GeV/c we remove the electron from this hypothesis list.

$$P(h|m;\Omega) \geq 0.10. \qquad (11)$$

The losses due to this cut are estimated by integration over the ionization distribution, for a given phase−space region Ω, of expression (10) with the condition (11). In the same way[2] it is possible to calculate the probability of misidentification (for example, pion as kaon) in order to account for "reflections" (sect. 2.6).

ISIS information is only used if it provides a sample of at least 100 good ionization measurements. This condition limits the identification capability of ISIS which mainly depends upon the relative longitudinal momentum of the particle, as shown in fig. 1.

2.4 π^0 − detection

The π^0's are detected in the Intermediate and Forward Gamma Detectors (IGD and FGD) of EHS [8] via their decay $\pi^0 \rightarrow \gamma\gamma$ (with branching ratio 98.8%). The $\gamma\gamma$ pair is requested to satisfy a kinematical one−constraint fit to the π^0 hypothesis with a probability larger than 4.5% using the assumption that the π^0 originates from the production vertex. The γ energy thresholds have been chosen (0.9 GeV in IGD and 2 GeV in FGD to maximize the signal to background ratio in the $\pi^0 \rightarrow \gamma\gamma$ region.

Very asymmetric decays $\pi^0 \rightarrow \gamma_1\ \gamma_2$ are rejected, using the condition $|\cos\Theta| \leq 0.9$, where $\cos\Theta = \frac{E_1 - E_2}{p_{\pi^0}}$, p_{π^0} is the π^0 momentum, and E_1, E_2 are the energies of the gammas.

The combined geometrical acceptance of the gamma detectors is presented in fig. 2. The valley observed at $Y^* \approx 2$ is due to the reduced γ detection efficiency at the geometrical intersection of IGD and FGD. Nevertheless, π^0 produced in the region $x_F \geq 0.01$ can be observed and used in the subsequent analysis.

In order to reduce the combinatorial background in the $\gamma\gamma$ invariant mass, showers due to charged hadrons have been rejected. This rejection leads to a loss of 3% of the π^0 signal but reduced the background by more than 20%.

An additional loss of π^0's comes from the limited two showers spatial resolution of the gamma detectors (d = 4cm for FGD and 10 cm for IGD): this loss is taken into account, using the relation $\sin\Theta^{min} \approx 2d \times M_{\pi^0}/P_{\pi^0}$.

Finally, losses due to conversion in the materials upstream of IGD and FGD are taken into account, including the conversion in the remaining hydrogen target, using the real position of the primary vertex.

The overall efficiency for π^0 detection and reconstruction in the kinematical region $x_F \geq 0.01$ is approximately 50% and the systematic error on π^0 total cross section is smaller than 6%.

The acceptance for resonances which includes a π^0 in its decay products has been limited in order to satisfy the following condition. For any polar angle ϕ_J defined by

---

[2] Actually, one has to calculate the minimum and maximum ionization ($I_{min} < I_m < I_{max}$) for which the condition (11) is satisfied.

$$\cos\phi_J = (\vec{n}_{beam} \times \vec{n}_{res})(\vec{n}_{\pi^0} \times \vec{n}_{res})$$

the π^0 is reconstructable if it corresponds to forward π^0 emission in the resonance decay system. This condition is satisfied if $x_F \geq 0.02$ for $\rho^{\pm}(770)$ and $x_F \geq 0.06$ for $\omega(783)$.

2.5 Fitting Procedure

The total and differential cross sections of vector meson resonances in reactions (1) to (6), are obtained by fits to the corresponding invariant mass distributions, i.e. $(\pi^-\pi^0)$ for $\rho^-(770)$, $(\pi^+\pi^-\pi^0)$ for $\omega(783)$, $(\pi^+\pi^0)$ for $\rho^+(770)$, $(K^+\pi^-)$ for $K^{*0}(892)$, $(K^-\pi^+)$ for $\overline{K}^{*0}(892)$ and (K^+K^-) for $\phi(1020)$. In fig. 3 are shown some typical mass distributions.

Depending on the relation between the natural resonance width (Γ_N) and the experimental resolution in the invariant mass ($\Gamma_R = FWHM$) the following three forms have been used for the fit:

(a) $\Gamma_N >> \Gamma_R$: ($\rho(770)$ and $K^*(892)$)

$$d\sigma/dM = BG(p^*) \times (1 + \beta \times BW(M)), \tag{12}$$

where $BW(M)$ is the relativistic P−wave Breit−Wigner function

$$BW(M) = \left(\frac{M}{p^*}\right) \times \frac{\Gamma_T}{(M^2 - M_R^2)^2 + (\Gamma_T M_R)^2)} \tag{13}$$

with

$$\Gamma_T = \Gamma_l + \Gamma_R, \quad \Gamma_l = \Gamma_N \times \left(\frac{M_R}{M}\right) \times \left(\frac{p^*}{p_R^*}\right)^3,$$

p^* is the momentum of the decay products in the resonance centre of mass, $p_R^* = p^*$ at the mass of the resonance M_R. The background is described by the form

$$BG(p^*) = \alpha_1 \left(\frac{p^*}{M}\right)^{\alpha_2} \times e^{-\alpha_3 p^* - \alpha_4 p^{*2}}. \tag{14}$$

α_i (i = 1 to 4) and β are fit parameters.

(b) $\Gamma_N \approx \Gamma_R$: ($\phi(1020)$) the Breit−Wigner distribution (12) is folded with a Gaussian invariant mass resolution function,

(c) $\Gamma_N << \Gamma_R$: ($\omega(783)$)

$$d\sigma/dM = BG(M) + \beta \frac{1}{\sqrt{2\pi\sigma^2}} e^{-\frac{(M - M_R)^2}{2\sigma^2}}, \tag{15}$$

where $\sigma = \Gamma_R/2.35$ and

$$BG(M) = \alpha_1(M - M_{th})^{\alpha_2} \times e^{-\alpha_3 M - \alpha_4 M^2}. \quad (16)$$

M_{th} is the 3π threshold mass.

2.6 Reflections

A well known difficulty arises when the particle identification efficiency is limited. Resonance signals (e.g.

$$K^*(892))$$

in the invariant mass spectrum for a particular particle combination (e.g. $K^+\pi^-$) are distorted by other (e.g.

$$\rho^0(770) \rightarrow \pi^+\pi^-$$

and

$$\overline{K}^{*0}(892) \rightarrow \pi^+ K^-)$$

combinations if a particle (e.g. π^+) is misidentified (e.g. as a K^+). This problem occurs for the phase space region where ISIS cannot provide efficient particle identification, i.e. for $K^{*0}(892)$ at $x_F > 0.5$.

The $K^{\pm}\pi^{\mp}$ invariant−mass spectra can be corrected for the $\rho(770)$ and $f_2(1270)$ reflection following the method of ref. [9]. For each $K\pi$ pair falling into a given x−interval we reassign the π mass to the particle which was previously assigned K−mass and, using the formalism [3] described above, we estimate the probability that it does not belong to the $\rho(770)$ and $f_2(1270)$:

$$W(M_{K\pi}) = (1 + \kappa \times \{\beta(\rho(770) \times BW_{\rho(770)}(M_{\pi\pi}) + \beta_2(f_2(1270) \times BW_{f_2(1270)}(M_{\pi\pi})\})^{-1},$$

where κ is the probability for the pion to satisfy the condition (11) for the kaon hypothesis. Using this probability as a weight for $K\pi$ combinations we can correct for the $\rho(770)$ and $f_2(1270)$ reflection.

We have checked that this method yields the same results as the standard one (using ISIS and no reflection subtraction) in the region ($0 < x_F < 0.2$) where particle identification is efficient.

---

[3] We neglected reflection of $K^*(892)$ into $\rho(770)$ because $\sigma(K^*(892)) << \sigma(\rho(770))$ for $x_F > 0.2$.

2.7 Resonance Parameters

As a check of the fitting procedure, we have left free, in a first attempt, the masses and widths of the $\phi(1020)$, $\omega(783)$ and $K^{*0}(892)$.

For the masses, we find $M(\phi) = (1019.4 \pm 0.6)MeV/c^2$, $M(\omega) = (782.0 \pm 3.0)MeV/c^2$ and $M(K^*)= (900.2 \pm 3.6)MeV/c^2$ to be compared to the PDG values [10]: 1019.5, 782.6 and 896.5 MeV/c^2, respectively.

For the widths, we find $\Gamma_I(\phi) = 9.5 \pm 1.7$ MeV/c^2, $\Gamma_I(\omega) = 33.9 \pm 6.8$ MeV/c^2 and $\Gamma_I(K^*)=(69.0 \pm 17.2)MeV/c^2$, for a mass resolution of 4.4, 35. and 15. MeV/c^2, respectively.

These results are in excellent agreement with the expected values. In the following, we shall fix all the masses and widths of the resonances to the PDG values [10].

3. RESULTS

The cross sections obtained for vector meson production for various x_F intervals are given in Table 1 on page 17 and figs 4−6. The errors quoted are statistical only. These cross sections take into account the branching ratios of the observed final states.

Concerning reactions (8) and (9), we can only quote an upper limit for $K^{*\pm}(892)$ production since no significant signal is observed in the channel $K^{*\pm} \rightarrow K^{\pm}\pi^0$

$$\sigma(K^{*-}) \leq 1.2^{+2.6}_{-0.8}\ mb,$$

$$\sigma(K^{*+}) \leq 0.5^{+3.8}_{-0.4}\ mb.$$

Before comparing with other results, it is worthwile to evaluate the losses due to the rejection of the two−prong events in our sample. The only channel which is affected by this rejection in a significant way is the $\rho^-(770)$ production at large x_F. Using simple isospin arguments, and the observed $\rho^0(770)$ production in four−prong event (0.49 ± 0.05 mb), one estimates the losses of $\rho^-(770)$ in the $0.5 \div 1.0$ x_F range to be (0.60 ± 0.10)mb.

Taking into account this correction, a comparison of our results with those obtained for π^+p interactions at 250 GeV/c, $x_F > 0.3$ [11] can be made (Table 2 on page 17). The agreement is excellent.

3.1 Vector meson production in the π^- fragmentation region

We now compare the production of vector mesons in the π^- fragmentation region, i.e. for $0.2 < x_F < 0.80$.

First, we note that

$$R_1 = \frac{\sigma(\rho^-)}{\sigma(\rho^0)} = 0.86 \pm 0.19. \quad (17)$$

In models where the incident valence quarks can recombine, one expects a ratio two to three times larger (the ρ^- contains two valence quarks identical to those of the π^-, the ρ^0 only one). This is notably the case of the additive quark model [12] and of the single string LUND model [13], which predicts a ratio $R_1 = 2.8$. In models which do not allow recombination, like the DTU model [14], one expects $R_1 = 1.4$, in better agreement with the observations. We conclude that the valence quark recombination does not propose a good interpretation of the data [9], [11].

The ratio

$$R_2 = \frac{\sigma(\rho^+)}{\sigma(\rho^0)} = 0.25 \pm 0.09 \quad (18)$$

is, as expected (the ρ^+ does not contain valence quarks identical to those of the π^-), smaller than one. Indeed all the string models predict R_2 values of the order of 0.4. The experimental result suggests a suppression of $\rho^+(770)$ beyond the current predictions of the string models.

The ratio obtained for

$$R_3 = \frac{\sigma(\omega)}{\sigma(\rho^0)} = 0.85 \pm 0.15 \quad (19)$$

indicates that I = 1 and I = 0 ($\bar{u}u \pm \bar{d}d$) combinations have a similar probability to be formed in the π^- fragmentaion region. This ratio differs significantly from the result obtained for π^+p interactions at 15.7 GeV/c $R_3 = 0.44 \pm 0.07$ which is obtained, however, when limiting the measurements to the sum of the exclusive channels [15]. This, however, was obtained by limiting the measurements to the sum of the exclusive channels.

The comparison of K^* to ρ production provides information on the strange quark suppression. In the π^- fragmentation region ($0.2 < x_F < 0.8$) we can estimate this value from comparison of K^{*0} to ρ^- whereas the comparison of

$$\overline{K}^{0*}$$

to ρ^+ may be related to the strange quark suppression factor in the sea (remember that

$$K^{*0} = d\bar{s}, \overline{K}^{*0} = \bar{d}s,$$

whereas $\rho^- = \bar{u}d$ and $\rho^+ = \bar{d}u$)

$$\lambda_s^{frag} = R_4 = \frac{\sigma(K^{*0})}{\sigma(\rho^-)} = 0.27 \pm 0.06, \quad (20)$$

$$\lambda_s^{sea} = R_5 = \frac{\sigma(\overline{K}^{*0})}{\sigma(\rho^+)} = 0.31 \pm 0.15. \quad (21)$$

The differential cross section for $\phi(1020)$ production is shown in fig. 6 and compared to the results obtained at 100 GeV/c (π^-Be interactions) [16]. The two results are in fair agreement, taking into account the large statistical errors which affect our results leads to comparing the $\phi(1020)$ production to the (non−strange quark) isoscalar vector meson ω production

$$R_6 = \frac{\sigma(\phi)}{\sigma(\omega)} = 0.048 \pm 0.015 \tag{22}$$

for $0.20 < x_F < 0.80$.

3.2 Test of the OZI suppression rule

R_6 can also be used to estimate the degree of suppression of unconnected to connected quark lines in the production of vector mesons (OZI suppression rule [17]). It is first necessary to estimate the fraction of $\phi(1020)$ which is not produced in association with particles containing strange quarks.

Using particle identification, we can estimate the fraction of the interactions where a $\phi(1020)$ is produced (at $x_F > -0.05$) in association with a K^+ or a K^- (at $x_F > -0.10$) to the total ϕ production

$$\frac{\sigma(\phi K^{\pm})}{\sigma(\phi)} = 0.70 \pm 0.10. \tag{23}$$

Assuming that half of the K, $\overline{K}$, and K^*, $\overline{K}^*$ produced in association with $\phi(1020)$ lead to a K^+ or K^-, one may now use expressions (22) and (23) to estimate the degree of OZI suppression for strange quarks

$$R_{OZI} = 0.014 \pm 0.006.$$

Very limited experimental information is available on the OZI suppression rule. One of the most accurate measurements has been obtained for $\bar{p}p$ annihilation in the (0.70 ÷ 0.76)GeV/c momentum range [18]:

$$R_{OZI} = \frac{\sigma(\bar{p}p \to \phi\pi^+\pi^-)}{\sigma(\bar{p}p \to \omega\pi^+\pi^-)} = 0.019 \pm 0.005.$$

The $\phi(1020)$ is not a pure $\bar{s}s$ state. The deviation from ideal mixing for the vector mesons (Θ = 39°) leads to the following expected ratio:

$$R_{OZI}^{TH} = tg^2(\Theta - \Theta_0) = 0.0034 \pm 0.0005.$$

One sees that for π^- fragmentation as well as for $\bar{p}p$ annihilation, the OZI suppression rule seems to be broken by dynamical effects [19].

3.3 Vector versus pseudo – scalar meson production

In a previous publication [7] we have reported results on ($\pi^{\pm}, \pi^0, K^{\pm}, \eta$ and η') inclusive production cross sections for $x_F > 0$. We can now use results on vector mesons production to estimate which fraction of the pseudo – scalar particles observed originates from the decay of vector mesons.

For this purpose we have to extrapolate the inclusive cross section for $\rho^+(770)$ and $\rho^-(770)$ from $x_F > 0.02$ to $x_F > 0.0$ and from $x_F > 0.06$ to $x_F > 0.0$ for $\omega(783)$ (as well as from $x_F > 0.10$ to $x_F > 0.0$ for η). The results of the extrapolation are shown in Table 3 on page 18, and the corresponding contributions to π^+, π^-, π^0, K^+ and K^- are

$$\pi^+ = 0.286\eta + \rho^+ + \rho^0 + 0.896\omega + 0.568 f_2 + \frac{2}{3}\overline{K}^{*0} + 0.149\phi =$$

$$= 16.1 mb\,(0.426\ of\ all\ \pi^+),$$

$$\pi^- = 0.286\eta + \rho^- + \rho^0 + 0.896\omega + 0.568 f_2 + \frac{2}{3}K^{*0} + 0.149\phi =$$

$$= 23.4 mb\,(0.476\ of\ all\ \pi^-),$$

$$\pi^0 = 1.194\eta + \rho^- + \rho^+ + 0.983\omega + 0.568 f_2 + 0.333\,(K^{*0} + \overline{K}^{*0}) + 0.149\phi =$$

$$= 25.4 mb\,(0.511\ of\ all\ \pi^0).$$

Obviously, 40 to 50% of the π^+, π^- and π^0 observed in the final state are from the decay of vector mesons. We can conclude that direct production of pseudoscalar mesons and those from the products of high mass mesons (mainly vector mesons).

Similarly, we can estimate the fraction of K^+ which come from $K^{*0} \to K^+\pi^-$ decay

$$\sigma(K^{*0} \to K^+\pi^-) / \sigma(K^+) = 0.40 \pm 0.03\,,$$

and K^- from $\overline{K}^{*0} \to K^-\pi^+$ decay

$$\sigma(\overline{K}^{*0} \to K^-\pi^+) / \sigma(K^-) = 0.25 \pm 0.04.$$

With these estimates, and using the fragmentation symmetry assumption

$$(\bar{u}_{\pi^-} \to K^{*-}) \approx (d_{\pi^-} \to K^{*0}),$$

$$\sigma(K^+ + K^-) \approx \sigma(K^0 + \bar{K}^0),\ \sigma(K^{*+} + K^{*-}) \approx \sigma(K^{*0} + \overline{K}^{*0}).$$

We obtain (neglecting $K_2^*(1420)$ production)

$$\sigma(K^{*0}, K^{*+}, \phi \to K^+) / \sigma(K^+) = 0.56 \pm 0.04\,,$$

and

$$\sigma(\overline{K}^{*0}, K^{*-}, \phi \rightarrow K^{-}) / \sigma(K^{-}) = 0.49 \pm 0.04 .$$

So that half of pseudo − scalar mesons, strange or not, are produced via vector mesons.

The strange vector meson production can also be compared to the "direct" strange pseudoscalar one. It is found to be equal to

$$V{:}PS = \sigma(K^{*0} + \overline{K}^{*0}) : \sigma_{direct}(K^{+} + K^{-}) = 1.04 \pm 0.10. \quad (24)$$

This result may be surprising: simple spin counting factor would have predicted a ratio V:PS = 3:1. Earlier estimations of this ratio, for $K^{+}p$ interactions at 32, 70 and 250 GeV/c were also found to be close to one [20], [21], [22].

4. CONCLUSIONS

We have found that the vector meson production is comparable to the direct pseudo − scalar production. The former contribute, with their decays products, to half of the $\pi^{\pm}, \pi^{0}, K^{\pm}$ observed in the final state: a good understanding of the "direct" particle production must therefore go via the measurement of the vector mesons.

The comparison of $\sigma(\rho^{-})$, $\sigma(\rho^{0})$ and $\sigma(\rho^{+})$ in the π^{-} fragmentation region underlines the role of the incident valence quarks in the hadronization procedure. The recombination of the valence quarks in a single hadron is not operative.

For a given combination of the valence quarks in the hadronization process, isospin 0 and 1 are on equal footing.

The strange quark suppression factor is found of the order (0.24 ± 0.04).

Disconnected quark line diagrams are suppressed as compared to connected ones (OZI rule) but, perhaps, less than (0.014 ± 0.006).

Acknowledgments

We would like to acknowledge the specialists of EHS and of the SPS, the painstaking work of the scanning staff at the collaborating laboratories. One of us (Y.F.) thanks CERN EP and DD staff, especially H. Klein and H.R. Renshall, for their help in the data production. Finally, we would like to thank the various funding agencies of our collaboration for making this work possible.

REFERENCES

1. M. Aguilar – Benitez et. al. Zeitschr. für Phys. C31 (1986) 491.
2. J.L. Bailly et al., Zeitschr. für Phys. C36 (1987) 545.
3. M. Aguilar – Benitez et. al., Nucl. Inst. and Meth. A258 (1987) 26.
4. A. Firestone et al., Phys. Rev. D14 (1976) 2902.
5. Yu. Fisjak et al., Minimum bias events from EHS, CERN/EP 87 – 137, Preprint IFVE 87 – 185 (1987).
6. W. Allison et al., Nucl. Inst. and Meth. 224 (1984) 396.
7. M. Aguilar – Benitez et al., Europhys. Lett., 4 (11) (1987) 1261.
8. B. Powell et al., Nucl. Inst. and Meth. 198 (1982) 217.
9. P.V. Chliapnikov et al., Phys. Lett. 130B (1983) 432.
10. Particle Data Group, M. Aguilar – Benitez et al., Phys. Lett. 170B (1986) 1.
11. M. Adamus et al., Phys. Lett. B183 (1987) 425.
12. V.V. Anisovich and V.M. Shekhter, Nucl. Phys. B55 (1973) 455.
13. T. Sjostrand, Comp. Phys. Comm. 227 (1982) 243.
14. A. Capella et. al., Zeitschr. für Phys. C3 (1980) 329.
    A.V. Batunin, A.K. Likhoded and A.N. Tolstenkov, Sov. J. Yad. Fiz. 42 (1985) 424;
    A.V. Batunin, A.K. Likhoded and V.A. Petrov, Sov. J. Yad. Fiz. 48 (1988) 525.
15. J. Ferguson et al., Phys. Rev. D36 (1987) 1964.
16. H. Dijkstra et al., Zeitschr. für Phys. C31 (1986) 375.
17. S. Okubo, Phys. Lett. 5 (1963) 165;
    G. Zweig, CERN/TH 401 and CERN/TH 412 (unpublished);
    J. Iizuka, Prog. Theor. Phys. Suppl. 37 – 38 (1966) 21.
18. A.M. Cooper et. al., Nucl. Phys. B146 (1978) 1.
19. A.M. Zaitzev et al., JETF Letters 23 (1976) 664.
20. I.A. Ajinenko et al., Zeitschr. für Phys. C23 (1984) 307;
    P.V. Chliapnikov et al., Zeitschr. für Phys. C12 (1982) 113.

REFERENCES (Cont'd)

21. E.A. De Wolf et al., Zeitschr. für Phys. C31 (1986) 13.

22. N.M. Agababyan et al., Zeitschr. für Phys. C41, 539, 1989;
A. De Roeck, Inclusive particle production in hadron − proton interactions at 250 GeV/c, Ph.D. thesis, Univ. of Antwerp (1988) unpublished.

TABLE CAPTIONS

TABLE 1 The vector meson cross sections (mb) for different Feynman $-$ x intervals.

TABLE 3 Non $-$ strange vector meson cross sections (mb) for Feynman $-$ x $>$ 0.3.

TABLE 4 Resonance cross sections (mb) extrapolated to the region x $>$ 0.

Table 1

	x – interval					
Resonance	0 ÷ 1	0.1 ÷ 1	0.2 ÷ 1	0.3 ÷ 1	0.5 ÷ 1	0.2 ÷ 0.8
$\rho^-(770)$		4.58 ± 0.52	2.59 ± 0.33	2.24 ± 0.24	0.73 ± 0.12	1.86 ÷ 0.33
$\rho^0(770)$	6.35 ± 0.24	4.15 ± 0.16	2.95 ± 0.11	2.24 ± 0.09	1.37 ± 0.06	2.17 ÷ 0.29
$\omega(783)$		2.80 ± 0.64	2.18 ± 0.53	1.06 ± 0.15	0.41 ± 0.05	1.84 ÷ 0.20
$\rho^+(770)$		0.83 ± 0.43	0.54 ± 0.18	0.17 ± 0.15		0.54 ÷ 0.18
$K^{0*}(892)$	1.77 ± 0.13	0.93 ± 0.10	0.56 ± 0.07	0.48 ± 0.08	0.25 ± 0.05	0.50 ÷ 0.07
$\bar{K}^{0*}(892)$	1.07 ± 0.15	0.31 ± 0.09	0.17 ± 0.06	0.02 ± 0.03		0.17 ÷ 0.06
$\phi(1020)$	0.22 ± 0.02	0.12 ± 0.02	.086 ± .023	.065 ± .018		0.086 ÷ 0.023

Table 2

Reaction	σ (mb)	Reaction	σ (mb)
$\pi^+p \to \rho^+ X$	2.80 ± 0.27	$\pi^-p \to \rho^- X$	2.84 ± 0.25
$\pi^+p \to \rho^0 X$	2.44 ± 0.18	$\pi^-p \to \rho^0 X$	2.24 ± 0.09
$\pi^+p \to \rho^- X$	0.26 ± 0.22	$\pi^-p \to \rho^+ X$	0.17 ± 0.15
$\pi^+p \to \omega X$	1.10 ± 0.25	$\pi^-p \to \omega X$	1.06 ± 0.15

Table 3

Resonance	σ (mb) (measured)	σ (mb) (extrapolated)
$\rho^-(770)$	7.72 ± 0.94	8.95
	$(x > 0.02)$	
$\rho^0(770)$	6.35 ± 0.24	6.35
	$(x > 0.0)$	
$\omega(783)$	3.91 ± 0.83	4.68
	$(x > 0.06)$	
$\rho^+(770)$	1.66 ± 0.78	2.17
	$(x > 0.02)$	
$f_2(1270)$	1.03 ± 0.22	1.03
	$(x > 0.0)$	
$\omega(783)$	3.91 ± 0.83	4.68
	$(x > 0.06)$	
η	3.1 ± 0.5	7.2
	$(x > 0.10)$	
η'	2.9 ± 1.4	
	$(x > 0.3)$	
K^0_*	1.77 ± 0.13	1.77
	$(x > 0.0)$	
$\bar{K}^0_*$	1.07 ± 0.15	1.07
	$(x > 0.0)$	
π^+	37.8 ± 0.21	37.8
	$(x > 0.0)$	
π^-	49.10 ± 0.27	49.20
	$(x > 0.0)$	
π^0	49.7 ± 1.5	49.7
	$(x > 0.0)$	
K^+	2.95 ± 0.13	2.95
	$(x > 0.0)$	
K^-	2.80 ± 0.12	2.80
	$(x > 0.0)$	

FIGURE CAPTIONS

Fig. 1 ISIS efficiency: the solid line gives the geometrical acceptance; the dash − dotted line fraction of $K^{\pm}$ lost; the dotted line the fraction of $\pi^{\pm}$ misidentified as $K^{\pm}$.

Fig. 2 Gamma detector geometrical efficiency for π^0 reconstruction as a function of the rapidity y^* and the transverse momentum p_T.

Fig. 3 Invariant mass spectra and result of the fits (curves): (a) K^+K^-, (b) $\pi^+\pi^-\pi^0$, (c) $\pi^-\pi^0$, (d) $\pi^+\pi^0$, (e) $K^+\pi^-$, and (f) $K^-\pi^+$ combinations. The curves on the figures correspond to the fits of the full distribution with the forms (12) −(15) and for the background only.

Fig. 4 Differential cross section for ρ^- (full dots), ρ^0 (crosses), ρ^+ (circles) and ω^0 (triangles).

Fig. 5 Differential cross section for K^{*0} (+) and $\overline{K}^{0*}$ (o).

Fig. 6 Differential cross section for $\Phi(1020)$ (+) compared to [16] (o).

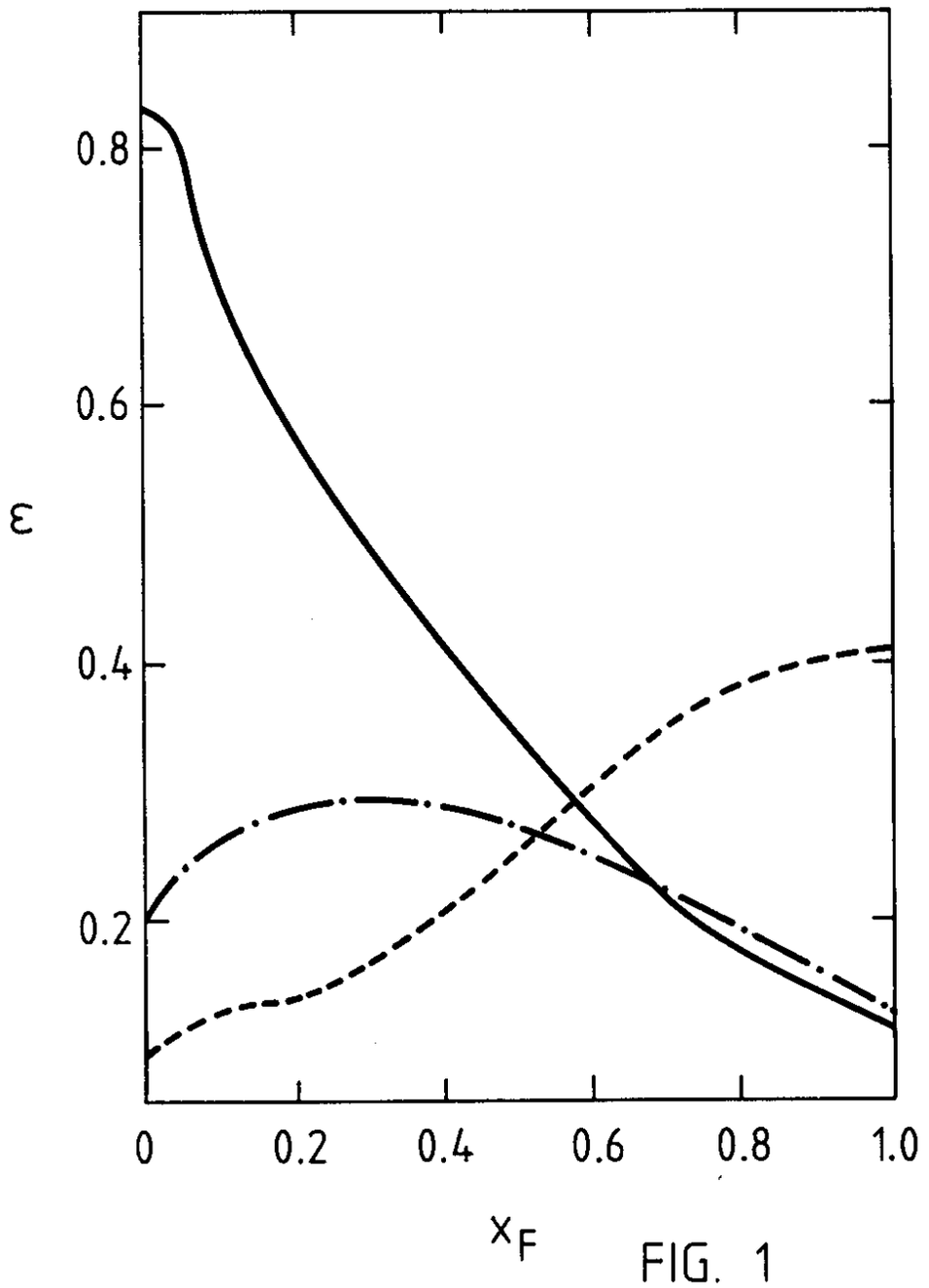

FIG. 1

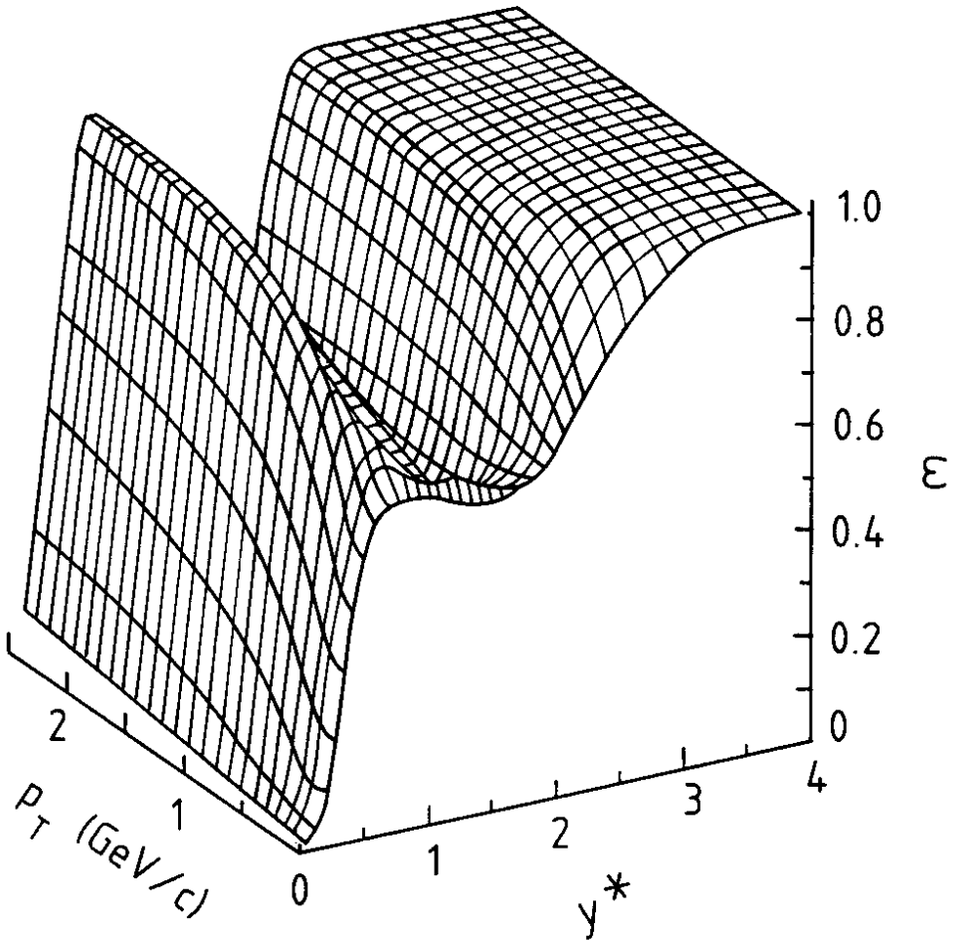

FIG. 2

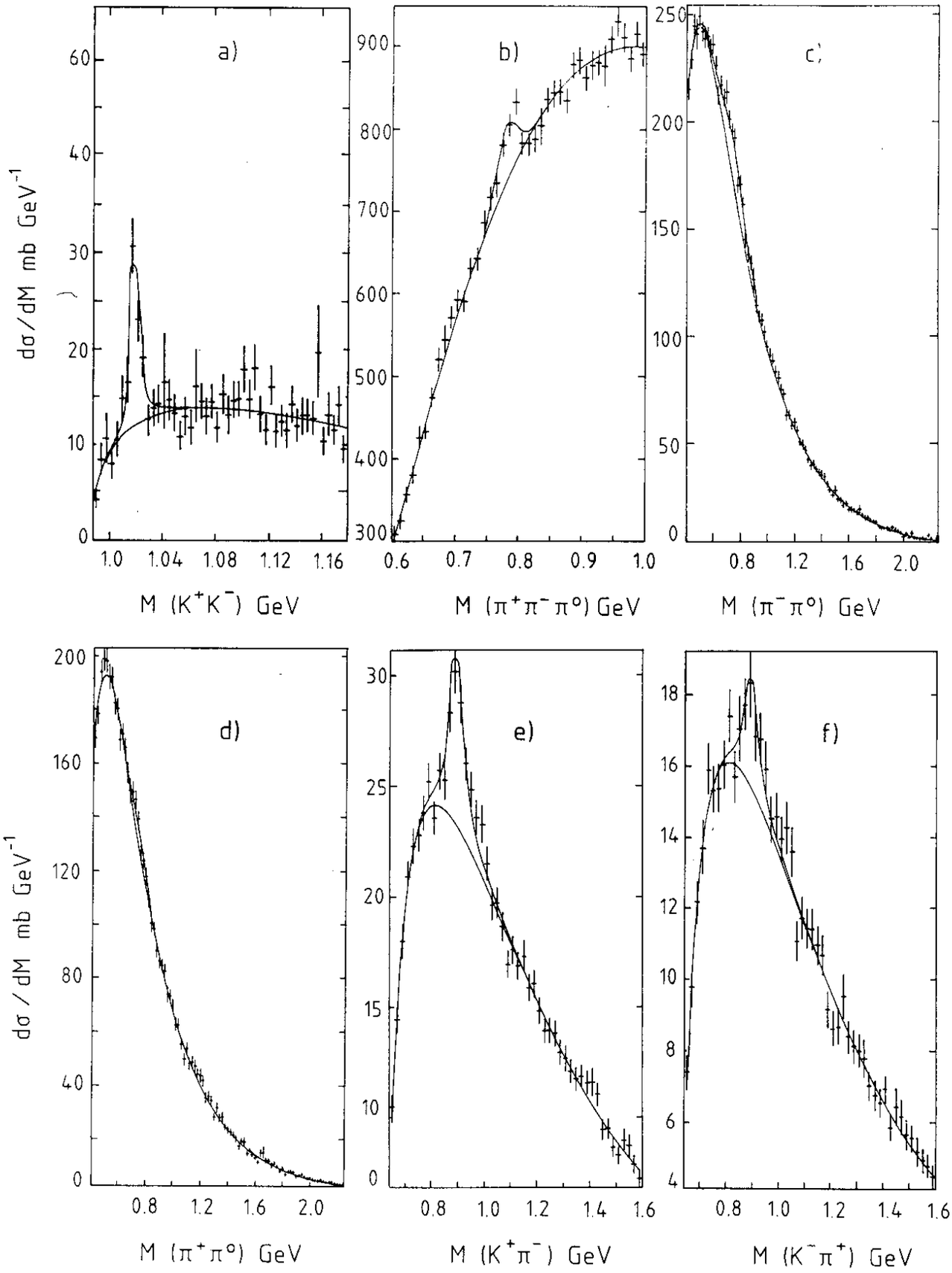
a)
b)
c)
d)
e)
f)
dσ/dM mb GeV⁻¹
M (K⁺K⁻) GeV
M (π⁺π⁻π°) GeV
M (π⁻π°) GeV
M (π⁺π°) GeV
M (K⁺π⁻) GeV
M (K⁻π⁺) GeV

FIG. 3

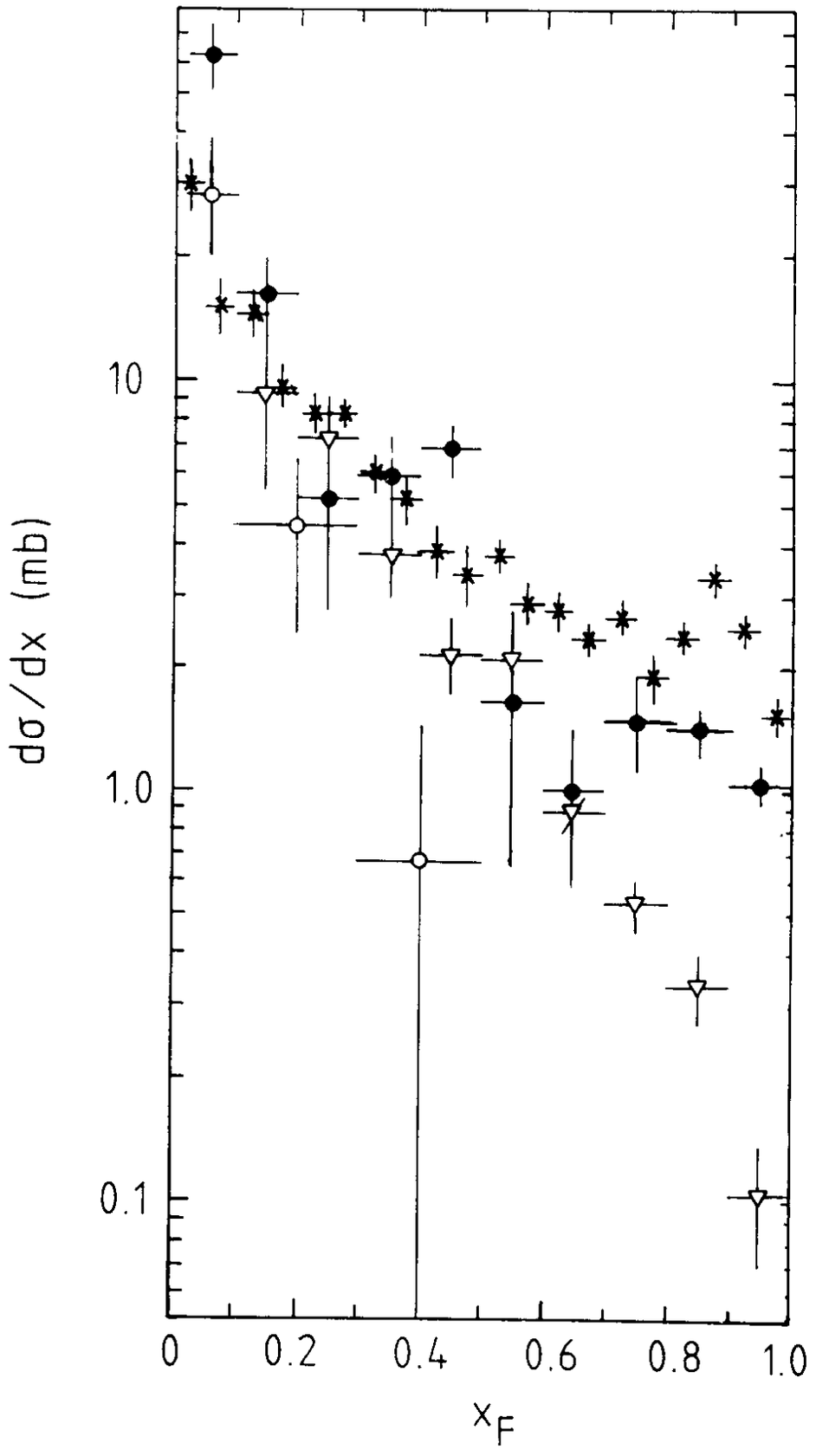

FIG. 4

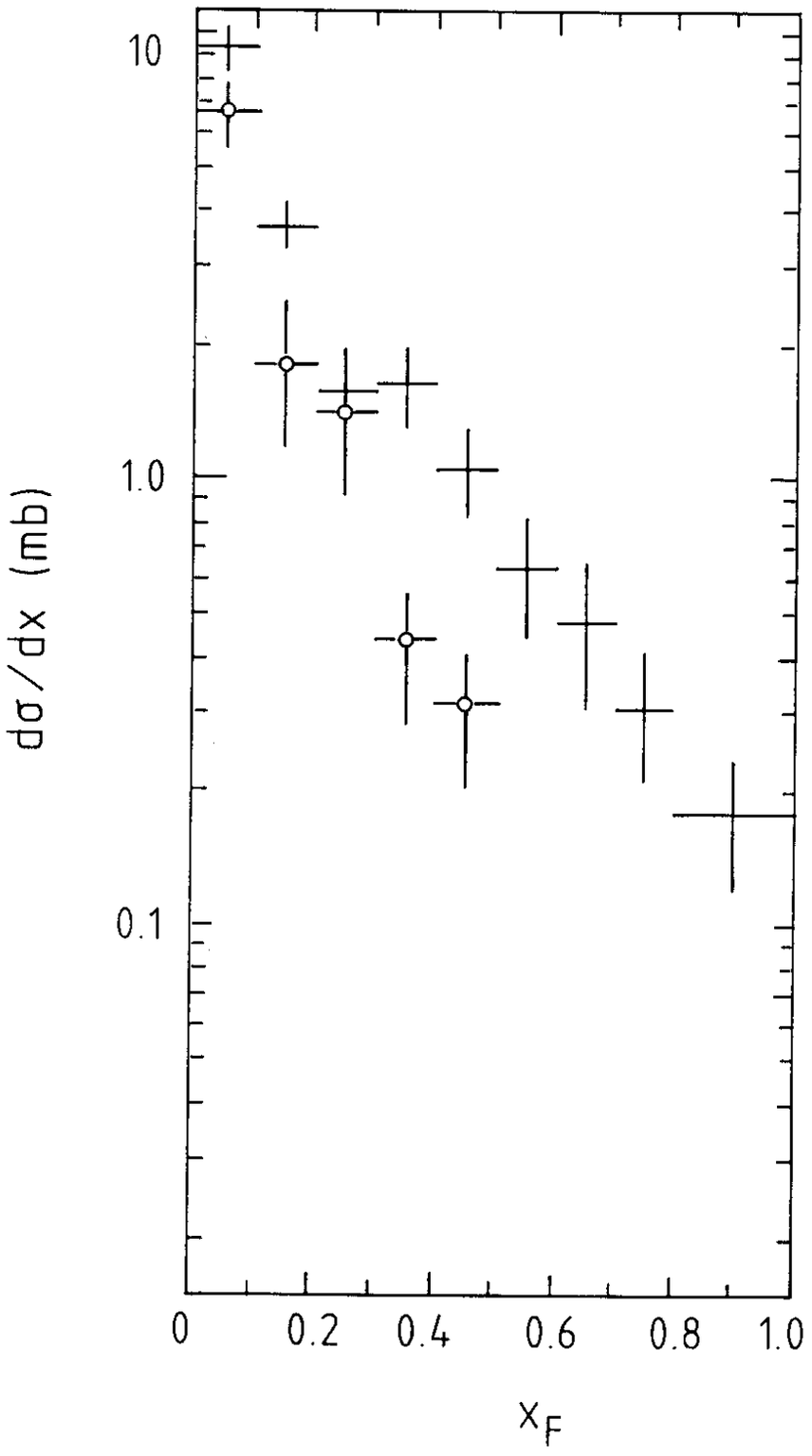

FIG. 5

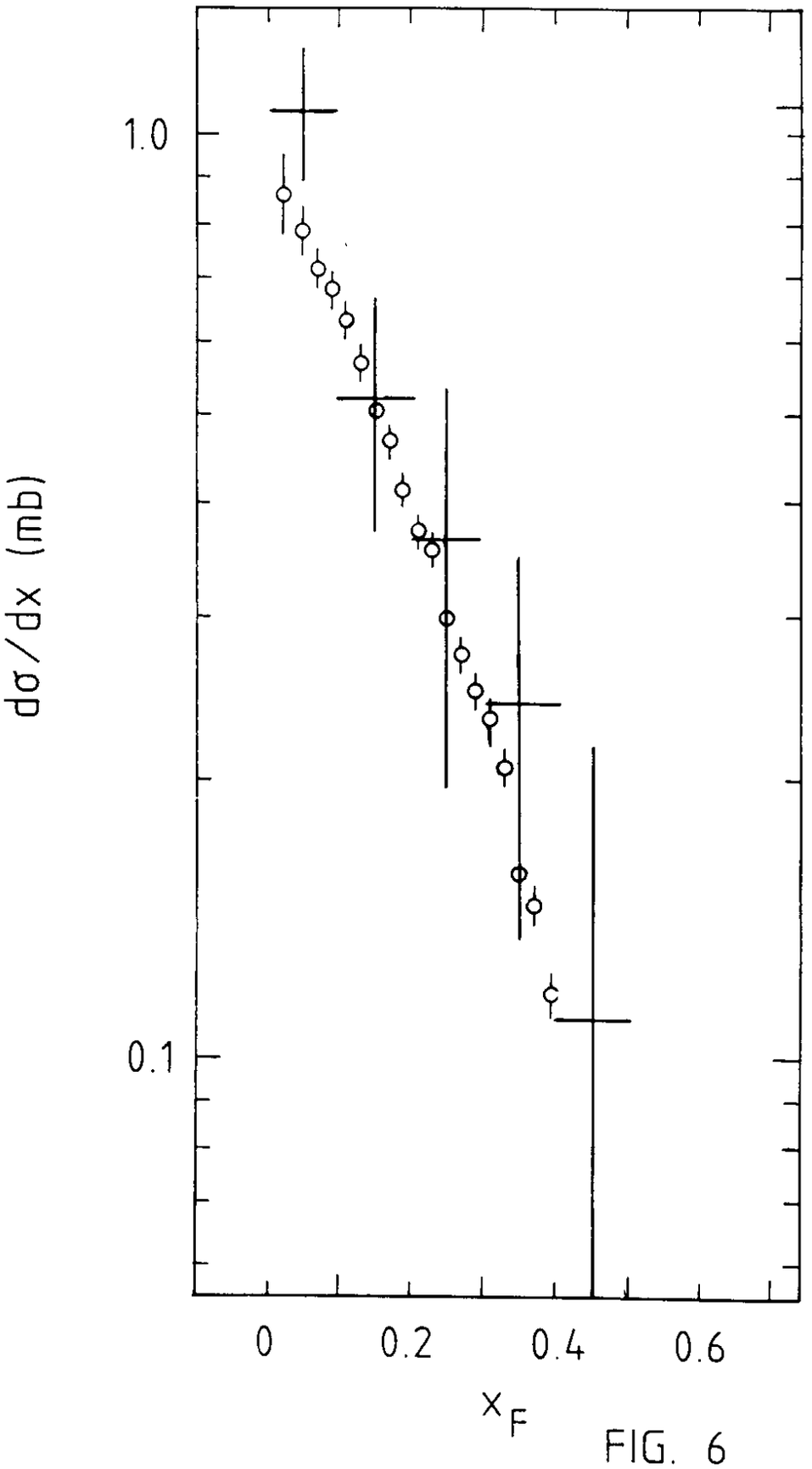

FIG. 6